Digital Signal Processing 69 (2017) 50–58

Contents lists available at ScienceDirect

Digital Signal Processing

www.elsevier.com/locate/dsp

On the asymptotic distribution of Time-Reversal MUSIC null spectrum

D. Ciuonzo [a,*], P. Salvo Rossi [b]

[a] Network Measurement and Monitoring (NM2) s.r.l., Centro Direzionale, Island E/7, 80143 Naples, Italy
[b] Department of Electronic Systems, Norwegian University of Science and Technology (NTNU), Trondheim, Norway

ARTICLE INFO

Article history:
Available online 20 June 2017

Keywords:
Time-Reversal (TR)
Radar imaging
Null-spectrum
Resolution
TR-MUSIC

ABSTRACT

In this paper we derive the asymptotic (viz. high signal-to-noise ratio) distribution of the null spectrum of the well-known Multiple Signal Classification (MUSIC) in its computational Time-Reversal (TR) form. The analysis builds upon classical results on the first-order perturbation of the singular value decomposition. These allow to obtain a simple characterization of the moments (up to the second order) of the spectrum and thus provide also a consistent form of the asymptotic "noisiness" measure in the TR case. The present study refers to a single-frequency case in a multistatic co-located scenario. The proposed analysis also enables a simple comparison of TR-MUSIC null-spectrum properties when linear and non linear (i.e. with mutual interaction effects) scattering models are assumed. Finally, a numerical analysis is provided to confirm the theoretical findings.

1. Introduction

1.1. Motivation and related works

Time-Reversal (TR) refers to all those methods exploiting the invariance of the wave equation (in stationary and lossless media) through time reversing with the intent of focusing on an emitting source or a scattering object. This is obtained by re-transmitting a time-reversed replica of the radiated/scattered field measured by an array of sensors and can be achieved physically [1] or in a computational fashion [2]. In the latter case (the so-called *computational* TR), the time-reversing procedure consists in back-propagating, by numerical means, the received data by using a known Green's function matched to the propagation medium. Since the representative Green function depends on the scattering object position, an image can be obtained by varying the probed scatterer location (the latter procedure is typically referred to as "imaging").

Therefore computational TR provides a useful tool to enable target detection/localization and represents the building rationale for imaging procedures in many applications, such as radar imaging [3], subsurface prospecting [4], through-the-wall imaging [5] and microwave imaging for early breast cancer detection [6–9].

The cornerstone of TR-imaging is represented by the so-called Multistatic Data Matrix (MDM), which collects the scattered field due to each Transmit–Receive (Tx–Rx) pair. Two popular methods for TR-imaging are represented by the decomposition of TR operator (DORT) and the TR Multiple Signal Classification (TR-MUSIC). More specifically, DORT imaging exploits the MDM spectrum by back-propagating separately the eigenvectors constituting the *signal subspace*. By doing so, selective focus on each (well-resolved) scatterer can be obtained [10].

On the other hand, TR-MUSIC is based on a complementary viewpoint with respect to DORT. Indeed, TR-MUSIC relies on the noise subspace, also referred to as orthogonal-subspace,[1] for the evaluation of the imaging function. The latter rationale leads to satisfactory performance as long as the signal subspace dimension does not occupy the entire data space dimension.

TR-MUSIC was first developed for a linear scattering model (that is, a Born Approximated (BA) model) [11]. Later, its successful application was also demonstrated for multiple scattering scenarios (i.e. in the presence of mutual interaction effects among the scatterers) [12]. Hence, TR MUSIC became very popular mainly due to: (*i*) algorithmic efficiency; (*ii*) no need for approximate scattering models; and (*iii*) finer resolution than the diffraction limits (especially for scenarios with few scatterers). Differently, for large number of scatterers (i.e. exceeding the Degrees Of Freedom (DOFs) associated to the corresponding spatial region), it has been shown that TR-MUSIC resolution ability deteriorates [13]. Recently, TR-MUSIC framework has been expanded to consider extended scatterers as well in [14].

* Corresponding author.
E-mail addresses: domenico.ciuonzo@ieee.org (D. Ciuonzo), salvorossi@ieee.org (P. Salvo Rossi).

[1] The term "orthogonal subspace" is commonly adopted to underline that the noise subspace is orthogonal to the signal subspace.

http://dx.doi.org/10.1016/j.dsp.2017.06.011

It is worth remarking that a huge literature on the performance analysis of MUSIC for Direction-Of-Arrival (DOA) estimation exists [15]. The development of MUSIC algorithm dates back to the pioneering work in [16]. A first performance study in terms of resolution was provided by [17] for a simple scenario, while a detailed analysis of MUSIC Mean Squared Error (MSE) can be found in the seminal works [18–21]. Theoretical performance analysis was later extended to array modeling errors both in terms of MSE (through a first-order perturbation approach) [22] and resolution [23]. The MSE/bias analysis in the presence of modeling errors was then obtained with the use of a second-order subspace perturbation approach in [24], while the resolution capability of MUSIC was studied under the same setup in [25]. Finally, a MSE/bias analysis, conditioned on the resolution event, was introduced in the recent work [26].

We underline that the aforementioned results do not have a direct application to TR-MUSIC. Indeed, in TR framework scatterers/sources are typically assumed unknown deterministic and more importantly a *single snapshot is used*, whereas MUSIC results for DOA refer to multiple snapshots and are often developed under different asymptotic (i.e., a very large number of snapshots) conditions. Additionally, up to authors' knowledge, *no corresponding theoretical studies have been proposed in the literature* for TR-MUSIC. The sole exception is represented by the works [27,28], providing the asymptotic localization MSE in the case point-like scatterers and thus tackling performance analysis of TR-MUSIC from a theoretical standpoint.

Yet, sub-optimal estimators were presented in [29,30] and compared in terms of localization performance based on Maximum-Likelihood Estimator (MLE) or tools from composite hypothesis testing, both for BA and *Foldy-Lax* (FL) (non-linear) models. The latter work employed however only simulation results for comparison. Differently, a theoretical performance study, based on the Cramér-Rao Lower Bound (CRLB), was presented in [31], considering both scattering models. Remarkably, the complementary task of estimating scattering potentials via a non-iterative (approximate) formula is addressed in [12] for generic location-only estimators.

1.2. Summary of the main contributions

In what follows, we summarize the main contributions of the present work:

- In this paper we are concerned with the performance of TR-MUSIC in the case of point-like scatterers with additive noise matrix corrupting data. To this end, we provide a performance analysis of TR-MUSIC null-spectrum in terms of its distribution. A co-located multistatic (narrowband) setup with either BA or FL scattering is considered in this paper.[2] The presented result is achieved via a first-order perturbation of Singular Value Decomposition (SVD). Then, the result holds asymptotically (viz. in the high Signal-to-Noise Ratio (SNR) regime).
- Our findings are complementary to those obtained in DOA literature for classic MUSIC [32] and can be used to highlight TR-MUSIC null-spectrum dependence on the measurement and scatterers configurations. In particular, the exact asymptotic distribution of the null spectrum is provided in this paper. Such result allows to obtain consistent estimates of both the mean and the variance of the null-spectrum, as well as to draw important considerations on the Normalized Standard Deviation (NSD), the latter being a measure of the *noisiness* of the spectrum. The aforementioned results are further exploited to provide a comparison of the asymptotic null-spectrum attained under both BA and FL models.
- Finally a few numerical examples, concerning simple scattering setups, are presented in order to validate the derived results. More specifically, we consider TR-MUSIC single-frequency space-space formulation for localizing scalar scatterers in a 2-D scenario.

[2] It is worth noticing that the proposed analysis hold for any general scattering (matrix) model whose functional map can be described in a deterministic fashion.

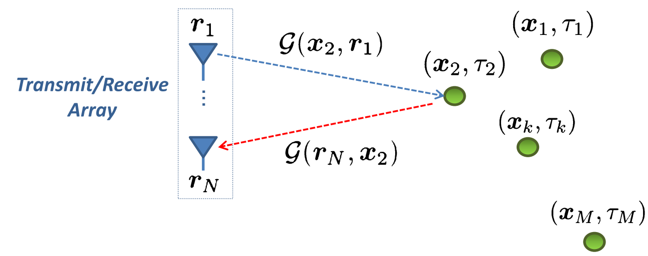

Fig. 1. System model for the considered co-located multistatic setup.

1.3. Paper organization and manuscript notation

The remainder of the manuscript is organized as follows: Sec. 2 describes the system model and reviews some classic results on SVD perturbation analysis. Sec. 3 presents the theoretical characterization of null-spectrum of TR-MUSIC algorithm, whereas these results are validated in Sec. 4 via simulations. Then, concluding remarks and further developments are reported in Sec. 5. Finally, technical proofs are deferred to the Appendix.

Notation – Lower-case (resp. Upper-case) bold letters denote column vectors (resp. matrices), with a_n (resp. $a_{n,m}$) being the nth (resp. the (n,m)th) element of $\boldsymbol{a}$ (resp. $\boldsymbol{A}$); $\mathbb{E}\{\cdot\}$, $\mathrm{var}\{\cdot\}$, $(\cdot)^T$, $(\cdot)^\dagger$, $\mathrm{Tr}[\cdot]$, $\mathrm{vec}(\cdot)$, $(\cdot)^-$, $\Re(\cdot)$, $\delta(\cdot)$, $\|\cdot\|_F$ and $\|\cdot\|$ denote expectation, variance, transpose, Hermitian, matrix trace, vectorization, pseudo-inverse, real part, Kronecker delta, Frobenius norm and ℓ_2 norm operators, respectively; $\mathbf{0}_{N\times M}$ (resp. $\boldsymbol{I}_N$) denotes the $N \times M$ null (resp. identity) matrix; $\mathbf{0}_N$ (resp. $\mathbf{1}_N$) denotes the null (resp. ones) vector of length N; $\mathrm{diag}(\boldsymbol{a})$ denotes the diagonal matrix obtained from the vector $\boldsymbol{a}$; $\boldsymbol{x}_{1:M}$ denotes the vector obtained by concatenation as $\boldsymbol{x}_{1:M} \triangleq \begin{bmatrix} \boldsymbol{x}_1^T & \cdots & \boldsymbol{x}_M^T \end{bmatrix}^T$; $\boldsymbol{\Sigma}_{\boldsymbol{x}}$ denotes the covariance matrix of the complex-valued random vector $\boldsymbol{x}$; $\mathcal{N}_{\mathbb{C}}(\boldsymbol{\mu}, \boldsymbol{\Sigma})$ denotes a proper complex Gaussian pdf with mean vector $\boldsymbol{\mu}$ and covariance matrix $\boldsymbol{\Sigma}$; $\mathcal{C}\chi_N^2$ denotes a complex chi-square distribution with N (complex) DOFs; finally the symbol $\sim$ means "distributed as".

2. System model

2.1. Signal model

The signal model is described hereinafter. We consider localization of point-like scatterers with a multistatic setup, as illustrated in Fig. 1. We assume that M point scatterers[3] are located at unknown positions $\{\boldsymbol{x}_k\}_{k=1}^M$ in $\mathbb{R}^p$ (where p represents the number of coordinates) with unknown scattering coefficients $\{\tau_k\}_{k=1}^M$ in $\mathbb{C}$. The Tx (resp. Rx) array consists of N isotropic point elements (resp. receivers) located at $\{\boldsymbol{r}_i\}_{i=1}^N$ in $\mathbb{R}^p$. The illuminators first send signals according to the scenario under consideration (i.e. in a known homogeneous background with wavenumber κ) and the transducer array records the received signals. The (single-frequency) measurement model is then [29]:

[3] The number of scatterers M is assumed known, as customary in array-processing literature [15].

$$\boldsymbol{K}_n = \boldsymbol{K}(\boldsymbol{x}_{1:M}, \boldsymbol{\tau}) + \boldsymbol{W} \tag{1}$$
$$= \boldsymbol{G}(\boldsymbol{x}_{1:M})\, \boldsymbol{M}(\boldsymbol{x}_{1:M}, \boldsymbol{\tau})\, \boldsymbol{G}(\boldsymbol{x}_{1:M})^T + \boldsymbol{W} \tag{2}$$

where $\boldsymbol{K}(\boldsymbol{x}_{1:M}, \boldsymbol{\tau}) \in \mathbb{C}^{N\times N}$ and $\boldsymbol{K}_n \in \mathbb{C}^{N\times N}$ denote the noise-free multistatic data matrix (MDM) in frequency-domain and the *measured* MDM, respectively. In Eq. (2), the (i, j)th element of the MDM corresponds to the scattered field detected at the ith transceiver in receive mode due to the unit excitation at the jth transceiver in transmit mode. Furthermore, $\boldsymbol{W} \in \mathbb{C}^{N\times N}$ is a noise matrix such that $\mathrm{vec}(\boldsymbol{W}) \sim \mathcal{N}_{\mathbb{C}}(\boldsymbol{0}_{N^2}, \sigma_w^2\, \boldsymbol{I}_{N^2})$. Additionally, we have denoted: (i) the vector of scattering coefficients as $\boldsymbol{\tau} \triangleq \begin{bmatrix} \tau_1 & \cdots & \tau_M \end{bmatrix}^T \in \mathbb{C}^{M\times 1}$; (ii) the Tx-Rx array matrix as $\boldsymbol{G}(\boldsymbol{x}_{1:M}) \in \mathbb{C}^{N\times M}$. The latter is defined explicitly as:

$$\boldsymbol{G}(\boldsymbol{x}_{1:M}) \triangleq \begin{bmatrix} \boldsymbol{g}(\boldsymbol{x}_1) & \boldsymbol{g}(\boldsymbol{x}_2) & \cdots & \boldsymbol{g}(\boldsymbol{x}_M) \end{bmatrix}. \tag{3}$$

In Eq. (3), $\boldsymbol{g}(\boldsymbol{x}) \in \mathbb{C}^{N\times 1}$ denotes the Tx-Rx Green's function vector as a function of the arbitrary location $\boldsymbol{x} \in \mathbb{R}^p$, that is:

$$\boldsymbol{g}(\boldsymbol{x}) \triangleq \begin{bmatrix} \mathcal{G}(\boldsymbol{r}_1, \boldsymbol{x}) & \mathcal{G}(\boldsymbol{r}_2, \boldsymbol{x}) & \cdots & \mathcal{G}(\boldsymbol{r}_N, \boldsymbol{x}) \end{bmatrix}^T. \tag{4}$$

It is worth noticing that the functional dependence of Eq. (4) is only due to $\mathcal{G}(\boldsymbol{x}', \boldsymbol{x})$, which denotes the *relevant* (scalar) background *Green function* [11]. Finally, in Eq. (2) the scattering matrix $\boldsymbol{M}(\boldsymbol{x}_{1:M}, \boldsymbol{\tau}) \in \mathbb{C}^{M\times M}$ for BA model [11] is defined as

$$\boldsymbol{M}(\boldsymbol{x}_{1:M}, \boldsymbol{\tau}) \triangleq \boldsymbol{T}(\boldsymbol{\tau}) = \mathrm{diag}(\boldsymbol{\tau}), \tag{5}$$

while in the case of FL model we have [31]

$$\boldsymbol{M}(\boldsymbol{x}_{1:M}, \boldsymbol{\tau}) \triangleq \left[\boldsymbol{T}^{-1}(\boldsymbol{\tau}) - \boldsymbol{S}(\boldsymbol{x}_{1:M})\right]^{-1}, \tag{6}$$

where the (m, n)th element of $\boldsymbol{S}(\boldsymbol{x}_{1:M})$ is defined as follows:

$$s_{m,n}(\boldsymbol{x}_{1:M}) \triangleq \begin{cases} \mathcal{G}(\boldsymbol{x}_m, \boldsymbol{x}_n) & m \neq n \\ 0 & m = n \end{cases}. \tag{7}$$

Our asymptotic analysis of TR-MUSIC null-spectrum distribution *is very general* and will account for both models in Eqs. (5) and (6).

Finally, to quantify the degree of mutual interaction (analogously to [12]), we employ the index

$$\eta \triangleq \frac{\|\boldsymbol{K}_{\mathrm{f}}(\boldsymbol{x}_{1:M}, \boldsymbol{\tau}) - \boldsymbol{K}_{\mathrm{b}}(\boldsymbol{x}_{1:M}, \boldsymbol{\tau})\|_F}{\|\boldsymbol{K}_{\mathrm{b}}(\boldsymbol{x}_{1:M}, \boldsymbol{\tau})\|_F}, \tag{8}$$

where $\boldsymbol{K}_{\mathrm{b}}(\boldsymbol{x}_{1:M}, \boldsymbol{\tau})$ and $\boldsymbol{K}_{\mathrm{f}}(\boldsymbol{x}_{1:M}, \boldsymbol{\tau})$ indicate the MDMs given in Eqs. (5) and (6), respectively. The aforementioned index will be employed in Sec. 4 to quantify the level of multiple scattering experienced in the considered numerical setups.

2.2. TR-MUSIC spectrum

TR-MUSIC is based on the evaluation of the *spatial spectrum* (also known as null-spectrum in DOA literature) [11]

$$\mathcal{P}(\boldsymbol{x}, \widetilde{\boldsymbol{U}}_n) \triangleq \left\| \widetilde{\boldsymbol{U}}_n^\dagger\, \bar{\boldsymbol{g}}(\boldsymbol{x}) \right\|^2 = \frac{\boldsymbol{g}(\boldsymbol{x})^\dagger\, \widetilde{\boldsymbol{P}}_n\, \boldsymbol{g}(\boldsymbol{x})}{\boldsymbol{g}(\boldsymbol{x})^\dagger\, \boldsymbol{g}(\boldsymbol{x})}, \tag{9}$$

where $\widetilde{\boldsymbol{U}}_n \in \mathbb{C}^{N\times(N-M)}$ is the matrix of left singular vectors of $\boldsymbol{K}_n$ corresponding to the noise subspace, $\bar{\boldsymbol{g}}(\boldsymbol{x}) \triangleq \boldsymbol{g}(\boldsymbol{x})/\|\boldsymbol{g}(\boldsymbol{x})\|$ is the unit-norm Green vector function and $\widetilde{\boldsymbol{P}}_n \triangleq (\widetilde{\boldsymbol{U}}_n \widetilde{\boldsymbol{U}}_n^\dagger)$ (i.e. the "noisy" projector into the left orthogonal subspace). It is worth noticing that TR-MUSIC in co-located case can be employed as long as the number of scatterers is lower than the number of Tx/Rx elements, i.e. $M < N$. It is apparent that Eq. (9) equals zero when $\boldsymbol{x}$ equals the true scatterers locations $\{\boldsymbol{x}_k\}_{k=1}^M$ in the noise-free case (i.e. when $\widetilde{\boldsymbol{U}}_n = \boldsymbol{U}_n$, the latter representing the matrix of eigenvectors corresponding to the left noise subspace of $\boldsymbol{K}(\boldsymbol{x}_{1:M}, \boldsymbol{\tau})$). For this reason, generally the M largest local maxima of $\mathcal{P}(\boldsymbol{x}, \widetilde{\boldsymbol{U}}_n)^{-1}$ are then chosen as the estimated positions $\{\hat{\boldsymbol{x}}_k\}_{k=1}^M$ [11].

2.3. SVD perturbation review

In what follows we provide preliminaries on first-order SVD perturbation, based on [33,34]. First, we consider a matrix $\boldsymbol{A} \in \mathbb{C}^{R\times T}$ with rank equal to $\delta < \min\{R, T\}$ (i.e. a rank deficient matrix). It can be easily shown that its SVD $\boldsymbol{A} = \boldsymbol{U}\,\boldsymbol{\Sigma}\,\boldsymbol{V}^\dagger$ can be rewritten as:

$$\boldsymbol{A} = \begin{pmatrix} \boldsymbol{U}_s & \boldsymbol{U}_n \end{pmatrix} \begin{pmatrix} \boldsymbol{\Sigma}_s & \boldsymbol{0}_{\delta\times\check{\delta}} \\ \boldsymbol{0}_{\bar{\delta}\times\delta} & \boldsymbol{0}_{\bar{\delta}\times\check{\delta}} \end{pmatrix} \begin{pmatrix} \boldsymbol{V}_s^\dagger \\ \boldsymbol{V}_n^\dagger \end{pmatrix}, \tag{10}$$

where $\bar{\delta} \triangleq (R-\delta)$ and $\check{\delta} \triangleq (T-\delta)$, respectively. Additionally, $\boldsymbol{U}_s \in \mathbb{C}^{R\times\delta}$ and $\boldsymbol{V}_s \in \mathbb{C}^{T\times\delta}$ (resp. $\boldsymbol{U}_n \in \mathbb{C}^{R\times\bar{\delta}}$ and $\boldsymbol{V}_n \in \mathbb{C}^{T\times\check{\delta}}$) have been used to denote the left and right unitary matrices of the signal subspace (resp. orthogonal subspace) in Eq. (10). We then consider a perturbed matrix $\widetilde{\boldsymbol{A}} = (\boldsymbol{A} + \boldsymbol{N})$, where $\boldsymbol{N}$ represents the perturbing term. Similarly as in Eq. (10), the SVD of $\widetilde{\boldsymbol{A}} = \widetilde{\boldsymbol{U}}\widetilde{\boldsymbol{\Sigma}}\widetilde{\boldsymbol{V}}^\dagger$ is rewritten as

$$\widetilde{\boldsymbol{A}} = \begin{pmatrix} \widetilde{\boldsymbol{U}}_s & \widetilde{\boldsymbol{U}}_n \end{pmatrix} \begin{pmatrix} \widetilde{\boldsymbol{\Sigma}}_s & \boldsymbol{0}_{\delta\times\check{\delta}} \\ \boldsymbol{0}_{\bar{\delta}\times\delta} & \widetilde{\boldsymbol{\Sigma}}_n \end{pmatrix} \begin{pmatrix} \widetilde{\boldsymbol{V}}_s^\dagger \\ \widetilde{\boldsymbol{V}}_n^\dagger \end{pmatrix} \tag{11}$$

which highlights the effect of $\boldsymbol{N}$ on the spectral representation of $\widetilde{\boldsymbol{A}}$. Indeed, differently from Eq. (10), $\widetilde{\boldsymbol{A}}$ may be *full-rank* in general. Additionally, Eq. (11) underlines the change of the left and right principal directions due to $\boldsymbol{N}$. This can be stressed as:

$$\widetilde{\boldsymbol{U}}_s = \boldsymbol{U}_s + \boldsymbol{\Delta}\boldsymbol{U}_s, \qquad \widetilde{\boldsymbol{U}}_n = \boldsymbol{U}_n + \boldsymbol{\Delta}\boldsymbol{U}_n, \tag{12}$$
$$\widetilde{\boldsymbol{V}}_s = \boldsymbol{V}_s + \boldsymbol{\Delta}\boldsymbol{V}_s, \qquad \widetilde{\boldsymbol{V}}_n = \boldsymbol{V}_n + \boldsymbol{\Delta}\boldsymbol{V}_n, \tag{13}$$

where $\boldsymbol{\Delta}(\cdot)$ terms in Eqs. (12) and (13) are in general complicated functions of $\boldsymbol{N}$. However, when $\boldsymbol{N}$ has a "small magnitude" (its meaning will be clarified hereinafter) compared to $\boldsymbol{A}$, a first-order perturbation (i.e. $\Delta(\cdot)$ are approximated as linear functions of $\boldsymbol{N}$), originally obtained in [35] and successively employed in DOA estimation in [20,33], will be accurate. Intuitively, a small perturbation is typically observed in the high Signal-to-Noise Ratio (SNR) regime, when $\boldsymbol{N}$ corresponds to a noise or disturbance matrix. In view of these considerations, next lemma will be used as the workhorse for our analysis.

Lemma. *The perturbed left orthogonal subspace $\widetilde{\boldsymbol{U}}_n$ (resp. right orthogonal subspace $\widetilde{\boldsymbol{V}}_n$) is spanned by $\boldsymbol{U}_n + \boldsymbol{U}_s\boldsymbol{B}$ (resp. $\boldsymbol{V}_n + \boldsymbol{V}_s\bar{\boldsymbol{B}}$) and the perturbed left signal subspace $\widetilde{\boldsymbol{U}}_s$ (resp. right signal subspace $\widetilde{\boldsymbol{V}}_s$) is spanned by $\boldsymbol{U}_s + \boldsymbol{U}_n\boldsymbol{C}$ (resp. $\boldsymbol{V}_s + \boldsymbol{V}_n\bar{\boldsymbol{C}}$), where matrices $\boldsymbol{B}$ and $\boldsymbol{C}$ (resp. $\bar{\boldsymbol{B}}$ and $\bar{\boldsymbol{C}}$) have norms of the order of that of $\boldsymbol{N}$. The adopted norm is required to verify the sub-multiplicative property (e.g. the Frobenius or ℓ_2 norms).*

The perturbations $\boldsymbol{\Delta}\boldsymbol{U}_n$ and $\boldsymbol{\Delta}\boldsymbol{V}_n$ have the following explicit expressions, valid up to the first order:

$$\boldsymbol{\Delta}\boldsymbol{U}_n = \boldsymbol{U}_s\,\boldsymbol{B} = -\boldsymbol{U}_s\,\boldsymbol{\Sigma}_s^{-1}\,\boldsymbol{V}_s^\dagger\,\boldsymbol{N}^\dagger\,\boldsymbol{U}_n; \tag{14}$$
$$\boldsymbol{\Delta}\boldsymbol{V}_n = \boldsymbol{V}_s\,\bar{\boldsymbol{B}} = -\boldsymbol{V}_s\,\boldsymbol{\Sigma}_s^{-1}\,\boldsymbol{U}_s^\dagger\,\boldsymbol{N}\,\boldsymbol{V}_n. \tag{15}$$

Correspondingly, $\boldsymbol{C} = -\boldsymbol{B}^\dagger$ and $\bar{\boldsymbol{C}} = -\bar{\boldsymbol{B}}^\dagger$ hold, thus giving:

$$\boldsymbol{\Delta}\boldsymbol{U}_s = \boldsymbol{U}_n\,\boldsymbol{C} = \boldsymbol{P}_{R,n}\,\boldsymbol{N}\,\boldsymbol{V}_s\,\boldsymbol{\Sigma}_s^{-1}; \tag{16}$$
$$\boldsymbol{\Delta}\boldsymbol{V}_s = \boldsymbol{V}_n\,\bar{\boldsymbol{C}} = \boldsymbol{P}_{T,n}\,\boldsymbol{N}^\dagger\,\boldsymbol{U}_s\,\boldsymbol{\Sigma}_s^{-1}. \tag{17}$$

In Eqs. (16) and (17) we have defined $\boldsymbol{P}_{R,n} \triangleq \boldsymbol{U}_n\boldsymbol{U}_n^\dagger$ and $\boldsymbol{P}_{T,n} \triangleq \boldsymbol{V}_n\boldsymbol{V}_n^\dagger$, respectively. Moreover, we remark that in obtaining Eqs. (14)–(17), "in-space" perturbation terms (e.g. the contribution of $\boldsymbol{\Delta}\boldsymbol{U}_n$ due to $\boldsymbol{U}_n$) are not taken into account, though they have been shown to be linear with $\boldsymbol{N}$ (i.e. *not negligible* at first-order).

The reason is that these terms do not affect performance analysis of TR-MUSIC null-spectrum when evaluated at scatterers positions $\boldsymbol{x}_k$, $k \in \{1, \ldots M\}$.

3. Null-spectrum analysis

3.1. General results

In this section we develop our high-SNR analysis of TR-MUSIC null-spectrum. To this end, we will exploit the results reviewed in Sec. 2.3 to the model introduced in Sec. 2.1 by adopting the correspondences (i) $\boldsymbol{A} \to \boldsymbol{K}(\boldsymbol{x}_{1:M}, \boldsymbol{\tau})$, (ii) $\boldsymbol{N} \to \boldsymbol{W}$ and (iii) $\widetilde{\boldsymbol{A}} \to \boldsymbol{K}_n$, respectively. First, we observe that the null-spectrum evaluated at scatterers locations $\mathcal{P}(\boldsymbol{x}_k, \widetilde{\boldsymbol{U}}_n)$, $k \in \{1, \ldots, M\}$ in Eq. (9) can be rewritten as

$$\mathcal{P}(\boldsymbol{x}_k, \widetilde{\boldsymbol{U}}_n) = \left\| (\boldsymbol{U}_n + \boldsymbol{\Delta U}_n)^\dagger \, \bar{\boldsymbol{g}}(\boldsymbol{x}_k) \right\|^2 \tag{18}$$

$$= \left\| \boldsymbol{\xi}_k \right\|^2 \tag{19}$$

exploiting the orthogonality property $\boldsymbol{U}_n^\dagger \, \bar{\boldsymbol{g}}(\boldsymbol{x}_k) = \boldsymbol{0}_{(N-M)}$ and the definition $\boldsymbol{\xi}_k \triangleq \boldsymbol{\Delta U}_n^\dagger \, \bar{\boldsymbol{g}}(\boldsymbol{x}_k)$. Therefore, in order to draw-out a statistical characterization of $\mathcal{P}(\boldsymbol{x}_k, \widetilde{\boldsymbol{U}}_n)$, we concentrate on the pdf of the random vector $\boldsymbol{\xi}_k$. Clearly, finding the exact distribution of $\boldsymbol{\xi}_k$ is a difficult task, as $\boldsymbol{\Delta U}_n$ is in general a complicated function on the unknown *perturbing* matrix $\boldsymbol{W}$.

However, $\boldsymbol{\Delta U}_n$ assumes a (tractable) closed form when a first-order approximation is considered (see Eq. (14)). This approximation holds tightly in the case of high SNR, as the matrix $\boldsymbol{W}$ will be statistically "small" (for a detailed discussion of this assumption see [35]) in comparison to noise-free MDM $\boldsymbol{K}(\boldsymbol{x}_{1:M}, \boldsymbol{\tau})$. Therefore, $\boldsymbol{\xi}_k$ is (approximately) expressed in terms of $\boldsymbol{W}$ (exploiting the result in Eq. (14)) as:

$$\boldsymbol{\xi}_k \approx -\boldsymbol{U}_n^\dagger \, \boldsymbol{W} \, \boldsymbol{V}_s \, \boldsymbol{\Sigma}_s^{-1} \boldsymbol{U}_s^\dagger \, \bar{\boldsymbol{g}}(\boldsymbol{x}_k) \,. \tag{20}$$

Thus the vector $\boldsymbol{\xi}_k$ is (approximately[4]) a linear function of the noise matrix $\boldsymbol{W}$, assumed in this manuscript statistically distributed according to a (complex) Gaussian distribution. Therefore, $\boldsymbol{\xi}_k$ will be Gaussian distributed too. Also, it is easy to show that $\boldsymbol{\xi}_k$ has a mean vector

$$\mathbb{E}\left\{\boldsymbol{\xi}_k\right\} = \boldsymbol{0}_{N-M} \,, \tag{21}$$

since $\mathbb{E}\{\boldsymbol{W}\} = \boldsymbol{0}_{N \times N}$. Differently, the closed-form of covariance $\boldsymbol{\Xi}_k$ is given by (since the mean is null)

$$\boldsymbol{\Xi}_k \triangleq \mathbb{E}\left\{\boldsymbol{\xi}_k \, \boldsymbol{\xi}_k^\dagger\right\} = \sigma_w^2 \, \|\boldsymbol{t}_k\|^2 \, \boldsymbol{I}_{N-M} \,, \tag{22}$$

where $\boldsymbol{t}_k \triangleq \boldsymbol{V}_s \, \boldsymbol{\Sigma}_s^{-1} \boldsymbol{U}_s^\dagger \, \bar{\boldsymbol{g}}(\boldsymbol{x}_k) \in \mathbb{C}^{N \times 1}$ is a *deterministic* vector, which also admits the more intuitive form:

$$\boldsymbol{t}_k = \boldsymbol{K}^{-}(\boldsymbol{x}_{1:M}, \boldsymbol{\tau}) \, \bar{\boldsymbol{g}}(\boldsymbol{x}_k) \,, \tag{23}$$

since we have exploited $\boldsymbol{K}^{-}(\boldsymbol{x}_{1:M}, \boldsymbol{\tau}) = \boldsymbol{V}_s \, \boldsymbol{\Sigma}_s^{-1} \boldsymbol{U}_s^\dagger \in \mathbb{C}^{N \times N}$ [36]. Finally, it is shown that the pseudo-covariance $\boldsymbol{\Psi}_k = \mathbb{E}\left\{\boldsymbol{\xi}_k \, \boldsymbol{\xi}_k^T\right\} = \boldsymbol{0}_{(N-M) \times (N-M)}$; therefore $\boldsymbol{\xi}_k$ is a *circular* complex Gaussian vector. The proof of both the aforementioned results is contained in the Appendix.

Therefore, in summary $\boldsymbol{\xi}_k$ is distributed as:

$$\boldsymbol{\xi}_k \sim \mathcal{N}_{\mathbb{C}}\left(\boldsymbol{0}_{N-M}, \|\boldsymbol{t}_k\|^2 \, \sigma_w^2 \, \boldsymbol{I}_{N-M}\right) \,. \tag{24}$$

Clearly, since $\boldsymbol{\xi}_k$ is a complex Gaussian with zero mean and diagonal covariance, its energy normalized by the variance of the generic component is distributed as follows:

$$\psi_k \triangleq \frac{\left\|\boldsymbol{\xi}_k\right\|^2}{\sigma_w^2 \, \|\boldsymbol{t}_k\|^2} \sim \mathcal{C}\chi^2_{N-M} \,. \tag{25}$$

In other terms, ψ_k is complex chi-square distributed with $N - M$ (complex) DOFs and with explicit pdf given by:

$$p_{\psi_k}(\psi) = \frac{\psi^{(N-M-1)}}{(N-M-1)\,!} \exp(-\psi), \quad \psi \geq 0 \,. \tag{26}$$

It is worth noticing that the DOFs of the obtained chi-square coincide with those available for TR-MUSIC localization properties. On the basis of the aforementioned result, it readily follows that

$$\mathbb{E}\left\{\left\|\boldsymbol{\xi}_k\right\|^2\right\} = \sigma_w^2 \, \|\boldsymbol{t}_k\|^2 \, \mathbb{E}\left\{\boldsymbol{\psi}_k\right\} \tag{27}$$

$$= \sigma_w^2 \, \|\boldsymbol{t}_k\|^2 \, (N-M) \,, \tag{28}$$

and

$$\mathrm{var}\left\{\left\|\boldsymbol{\xi}_k\right\|^2\right\} = \sigma_w^4 \, \|\boldsymbol{t}_k\|^4 \, \mathrm{var}\left\{\boldsymbol{\psi}_k\right\} \tag{29}$$

$$= \sigma_w^4 \, \|\boldsymbol{t}_k\|^4 \, (N-M) \,. \tag{30}$$

Therefore, we have obtained the mean and the variance of the pseudo-spectrum $\mathcal{P}(\boldsymbol{x}_k, \widetilde{\boldsymbol{U}}_n) = \left\|\boldsymbol{\xi}_k\right\|^2$. Also, by considering the Normalized Standard Deviation (NSD) [32,37] of the null-spectrum, we obtain:

$$\mathrm{NSD}_k \triangleq \frac{\sqrt{\mathrm{var}\left\{\mathcal{P}(\boldsymbol{x}_k, \widetilde{\boldsymbol{U}}_n)\right\}}}{\mathbb{E}\left\{\mathcal{P}(\boldsymbol{x}_k, \widetilde{\boldsymbol{U}}_n)\right\}} = \frac{1}{\sqrt{N-M}} \,. \tag{31}$$

It is apparent that the NSD *does not depend* (at high SNR) on the scatterers configuration and coefficients, as well as the noise power, but only on the (complex) DOFs, being equal to $N - M$. Therefore, the NSD becomes (asymptotically) very small *only* when the number of scatterers is few compared to the elements of the array.

First Remark: we recall that in [17] Kaveh and Barabell analyzed the performance of MUSIC for DOA estimation, focusing on the resolution property in the case of *two* closely-spaced emitters. In the aforementioned work the prerequisite for the proposed analysis to hold is that the standard deviation of $\mathcal{P}(\boldsymbol{x}_k, \widetilde{\boldsymbol{U}}_n)$ should be small compared to $\mathbb{E}\left\{\mathcal{P}(\boldsymbol{x}_k, \widetilde{\boldsymbol{U}}_n)\right\}$, $k \in \{1, 2\}$, so that the null-spectrum mean reflects the value of the random variable $\mathcal{P}(\boldsymbol{x}_k, \widetilde{\boldsymbol{U}}_n)$. Clearly, this assumption corresponds to:

$$\mathrm{NSD}_k \ll 1 \quad k \in \{1, 2\}. \tag{32}$$

Therefore, aiming at fostering a similar analysis to [17] for the TR setup, we will need that (32) holds true. This implies that two conditions need to be met. First, a sufficiently high SNR should be experienced in order for the proposed approximation to hold (recall that this is needed so that the first-order SVD perturbation is accurate). Secondly, when the SNR is sufficiently high, it is apparent from (31) that a further SNR increase does not improve the *stability* of the spectrum, but only an increase of the array aperture N does. Indeed the (asymptotic) NSD, being a measure of the noisiness of the null spectrum, is not dependent on the SNR. Remarkably, the aforementioned conditions have a strong analogy with the DOA case, where the asymptotic regime is achieved with a sufficient number of observed samples and a good spectrum (asymptotic) stability can be only obtained with increased (passive) receive array aperture [32].

Second Remark: in case the evaluated position of TR-MUSIC null-spectrum $\boldsymbol{x}$ does not coincide with one of the scatterers positions

[4] In the following of the manuscript we will omit the terms "approximated" and "approximately" implicitly referring to a high-SNR regime.

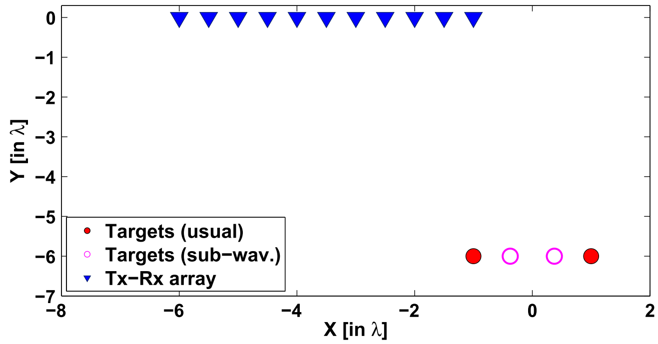

Fig. 2. Considered 2-D measurement/scatterers geometry; red filled "∘" markers correspond to a *usual* setup, while magenta "∘" markers to a *sub-wavelength* experiment. (For interpretation of the references to color in this figure legend, the reader is referred to the web version of this article.)

$\boldsymbol{x}_k$, $k \in \{1, \ldots, M\}$, it is apparent that the first term in the right-hand side of Eq. (18) is *not null* (i.e. $\boldsymbol{U}_n^\dagger \, \bar{\boldsymbol{g}}(\boldsymbol{x}) \neq \boldsymbol{0}_{N-M}$). Nonetheless, we observe that the preceding analysis can be still applied. Indeed, it can be readily shown that $\mathcal{P}(\boldsymbol{x}, \widetilde{\boldsymbol{U}}_n) = \|\boldsymbol{\xi}(\boldsymbol{x})\|^2$, where (in *approximated* sense[5]):

$$\boldsymbol{\xi}(\boldsymbol{x}) \sim \mathcal{N}_{\mathbb{C}}\left(\boldsymbol{U}_n^\dagger \, \bar{\boldsymbol{g}}(\boldsymbol{x}), \, \sigma_w^2 \, \|\boldsymbol{t}(\boldsymbol{x})\|^2 \, \boldsymbol{I}_{N-M}\right), \tag{33}$$

where we have similarly defined $\boldsymbol{t}(\boldsymbol{x}) \triangleq \boldsymbol{K}^-(\boldsymbol{x}_{1:M}, \boldsymbol{\tau}) \, \bar{\boldsymbol{g}}(\boldsymbol{x})$.

The aforementioned two remarks are deemed to be useful in order to provide a complete resolution threshold analysis, similarly to that developed for studying resolution capabilities of MUSIC in DOA estimation [17,37]. Indeed, with reference to TR applications, a similar rigorous analysis seems to be lacking in the literature at the present moment (up to the authors knowledge), except for some special setups [38]. The present objective falls however outside the scope of this manuscript and will be object of future studies.

3.2. BA vs. FL scattering models

Hereinafter we will compare the obtained theoretical results of TR-MUSIC null-spectrum with BA and FL models,[6] in order to investigate dependence of spectrum stability on a particular scattering model. First, we consider the ratio of the means (cf. Eq. (28))

$$\frac{\mathbb{E}\left\{\left\|\boldsymbol{\xi}_{k,\mathrm{f}}\right\|^2\right\}}{\mathbb{E}\left\{\left\|\boldsymbol{\xi}_{k,\mathrm{b}}\right\|^2\right\}} = \frac{\left\|\boldsymbol{K}_{\mathrm{f}}^-(\boldsymbol{x}_{1:M}, \boldsymbol{\tau}) \, \boldsymbol{g}(\boldsymbol{x}_k)\right\|^2}{\left\|\boldsymbol{K}_{\mathrm{b}}^-(\boldsymbol{x}_{1:M}, \boldsymbol{\tau}) \, \boldsymbol{g}(\boldsymbol{x}_k)\right\|^2} \triangleq \varsigma_k, \tag{34}$$

where the subscript "f" (resp. "b") refers to the corresponding quantity under FL (resp. BA) model. Similarly, the ratio among the variances is given by:

$$\frac{\mathrm{var}\left\{\left\|\boldsymbol{\xi}_{k,\mathrm{f}}\right\|^2\right\}}{\mathrm{var}\left\{\left\|\boldsymbol{\xi}_{k,\mathrm{b}}\right\|^2\right\}} = \varsigma_k^2 \,. \tag{35}$$

Therefore the coefficient ς_k determines *both* the ratio between the means and the variances. Interestingly, it is worth noticing that

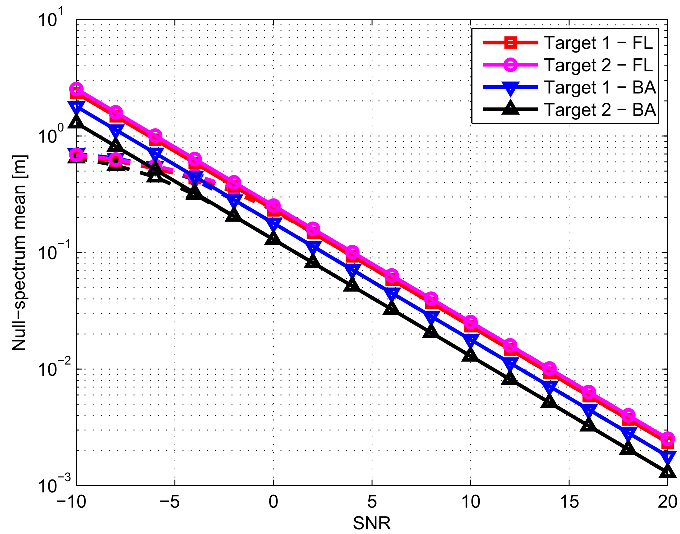

Fig. 3. TR-MUSIC null-spectrum in *usual* setup: Mean vs. SNR; theoretical (obtained via Eq. (28), in solid lines) vs. simulated (MC-based) performance.

the aforementioned term also dictates the relative performance between the MSE performance under the two scattering models. Indeed, ς_k also coincides with the ratio of the traces of the MSE matrices associated to FL and BA models, as shown in [28]. Also, after some manipulations, we can express the aforementioned coefficient as [28]:

$$\varsigma_k = \frac{\sum_{m=1}^{M} \lambda_{\mathrm{f},m}^{-1} \left\|\boldsymbol{u}_{s,\mathrm{f},m}^\dagger \, \boldsymbol{g}(\boldsymbol{x}_k)\right\|^2}{\sum_{m=1}^{M} \lambda_{\mathrm{b},m}^{-1} \left\|\boldsymbol{u}_{s,\mathrm{b},m}^\dagger \, \boldsymbol{g}(\boldsymbol{x}_k)\right\|^2}, \tag{36}$$

where $\boldsymbol{K}_{\mathrm{b}}(\boldsymbol{x}_{1:M}, \boldsymbol{\tau}) = (\boldsymbol{U}_{s,\mathrm{b}} \boldsymbol{\Sigma}_{s,\mathrm{b}} \boldsymbol{V}_{s,\mathrm{b}}^\dagger)$ (resp. $\boldsymbol{K}_{\mathrm{f}}(\boldsymbol{x}_{1:M}, \boldsymbol{\tau}) = (\boldsymbol{U}_{s,\mathrm{f}} \boldsymbol{\Sigma}_{s,\mathrm{f}} \boldsymbol{V}_{s,\mathrm{f}}^\dagger)$) is the SVD of MDM with BA (resp. FL) FL model. Also, in Eq. (36) we denoted $\lambda_{\mathrm{b},m}$ and $\boldsymbol{u}_{s,\mathrm{b},m}$ (resp. $\lambda_{\mathrm{f},m}$ and $\boldsymbol{u}_{s,\mathrm{f},m}$) as the mth eigenvalue of the *TR operator* $\boldsymbol{K}_{\mathrm{b}}^\dagger \boldsymbol{K}_{\mathrm{b}}$ (resp. $\boldsymbol{K}_{\mathrm{f}}^\dagger \boldsymbol{K}_{\mathrm{f}}$) [11] and the mth column of $\boldsymbol{U}_{s,\mathrm{b}}$ (resp. $\boldsymbol{U}_{s,\mathrm{f}}$), respectively.

However, by looking at the NSD obtained in Eq. (31), it is apparent that the latter measure is *independent* on the specific scattering model being considered. Therefore, it can be concluded that the stability of TR-MUSIC null-spectrum is independent on the specific scattering model being considered.

4. Numerical results

This section is devoted to confirm theoretical results of Sec. 3 via simulated results. Hereinafter we will restrict our attention to 2-D localization problems in a homogeneous background. In the latter case the relevant Green function is $\mathcal{G}(\boldsymbol{x}', \boldsymbol{x}) = H_0^{(1)}\left(\kappa \left\|\boldsymbol{x}' - \boldsymbol{x}\right\|\right)$ (we neglect the irrelevant constant scaling factor $\frac{j}{4}$), with $H_n^{(1)}(\cdot)$ and $\kappa = \frac{2\pi}{\lambda}$ denoting the nth order *Hankel* function of the first kind and the wavenumber (λ is the wavelength), respectively.

Also, we define $\mathrm{SNR} \triangleq \frac{\|\boldsymbol{K}(\boldsymbol{x}_{1:M}, \boldsymbol{\tau})\|_F^2}{N^2 \, \sigma_w^2}$ and we consider a multi-static scenario where $\lambda = 1$ (thus $\kappa = 2\pi$) and a $\frac{\lambda}{2}$-spaced Tx/Rx array of $N = 11$ elements is employed, as shown in Fig. 2. For the sake of simplicity, our examples refer to $M = 2$ targets within the investigated area. Finally, we will consider both *usual* (the distance between the scatterers is above λ) and *sub-wavelength* (the distance between the scatterers is under λ) setups in what follows (see Fig. 2).

Usual setup – Null-spectrum analysis: We first assume that the targets have coordinates $\boldsymbol{x}_1 = \begin{bmatrix} -1 & -6 \end{bmatrix}^T$ and $\boldsymbol{x}_2 = \begin{bmatrix} +1 & -6 \end{bmatrix}^T$

[5] We recall that, as explained in Sec. 2.3, we have ignored the linear "in-space" perturbation terms in the first-order SVD expansion, as they do not affect performance when $\boldsymbol{x} = \boldsymbol{x}_k$, $k \in \mathcal{K}$. However, in the case the considered position $\boldsymbol{x} \neq \boldsymbol{x}_k$, $k \in \mathcal{K}$, they are not exactly null and their contribution to asymptotic analysis should be validated. However, the present analysis is outside the scope of the present manuscript.

[6] Hereinafter, for simplicity, we will consider the expressions obtained holding with equality assuming we are in a high-SNR regime.

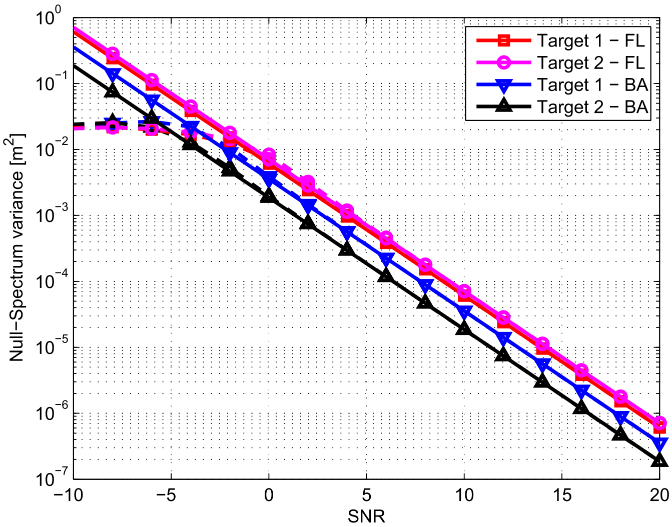

Fig. 4. TR-MUSIC null-spectrum in *usual* setup: Variance vs. SNR; theoretical (obtained via Eq. (30), in solid lines) vs. simulated (MC-based) performance.

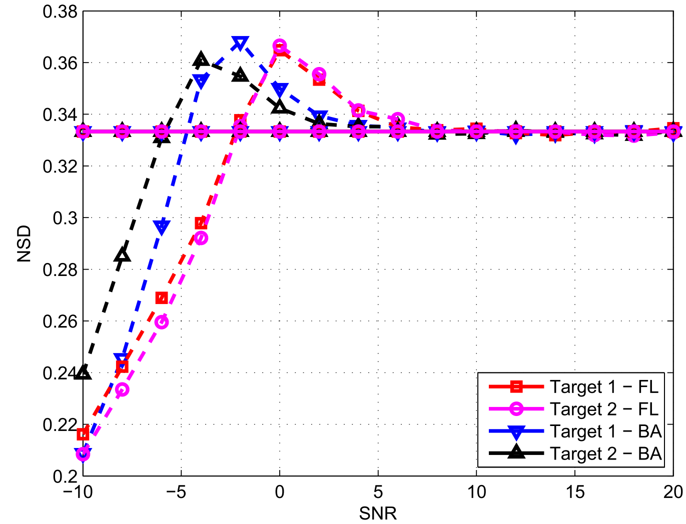

Fig. 5. TR-MUSIC null-spectrum in *usual* setup: NSD vs. SNR; theoretical (obtained via Eq. (31), in solid lines) vs. simulated (MC-based) performance.

(i.e. the distance between the scatterers is 2λ) and scattering coefficients $\boldsymbol{\tau} = \begin{bmatrix} 3 & 4 \end{bmatrix}^T$; in this case we have $\eta = (0.8232)$. Then, we compare the asymptotic expressions of the mean (28), variance (30), NSD (31) and pdf (25) with the true ones obtained by means of Monte Carlo (MC) simulation, obtained through 10^5 independent runs. Fig. 3 depicts the null-spectrum mean behavior vs. the SNR for the two targets being considered, both for FL and BA models. MC-based means are reported in dashed lines while the high-SNR theoretical approximations in solid lines. It is apparent that, as the SNR increases, the obtained result tightly approximate the mean expression. A similar conclusion can be drawn in Fig. 4 with reference to the trend of the variance vs. SNR. It is seen that both approximations can be deemed extremely accurate above the value SNR ≈ 2 dB. Consequently, as shown in Fig. 5, at the same SNR value the empirical NSD approaches the steady state value dictated by Eq. (31), which, for the present case equals $\frac{1}{\sqrt{11-2}} \approx 0.33$. Finally, in order to verify the convergence in distribution established by Eq. (25), we report in Fig. 6 the histograms of ψ_k for three representative SNR values (i.e., SNR $\in \{-6, -4, -2\}$ dB for BA scenario and SNR $\in \{-4, -2, 0\}$ dB for FL scenario) in comparison to the theoretical pdf given by Eq. (26). It is apparent that a similar SNR value as for mean and variance is required to ensure convergence to the asymptotic pdf provided.

Sub-wavelength setup – Null-spectrum analysis: Differently, in Figs. 7–10 we report a setup where we have set $\boldsymbol{x}_1 = \begin{bmatrix} -3/8 & -6 \end{bmatrix}^T$, $\boldsymbol{x}_2 = \begin{bmatrix} +3/8 & -6 \end{bmatrix}^T$ (see Fig. 2) and $\boldsymbol{\tau} = \begin{bmatrix} 3 & 5 \end{bmatrix}^T$. This scenario constitutes a *sub-wavelength* experiment, since the distance between the scatterers is $\frac{3}{4}\lambda$. Clearly, in this case $\eta = (1.5706)$, which

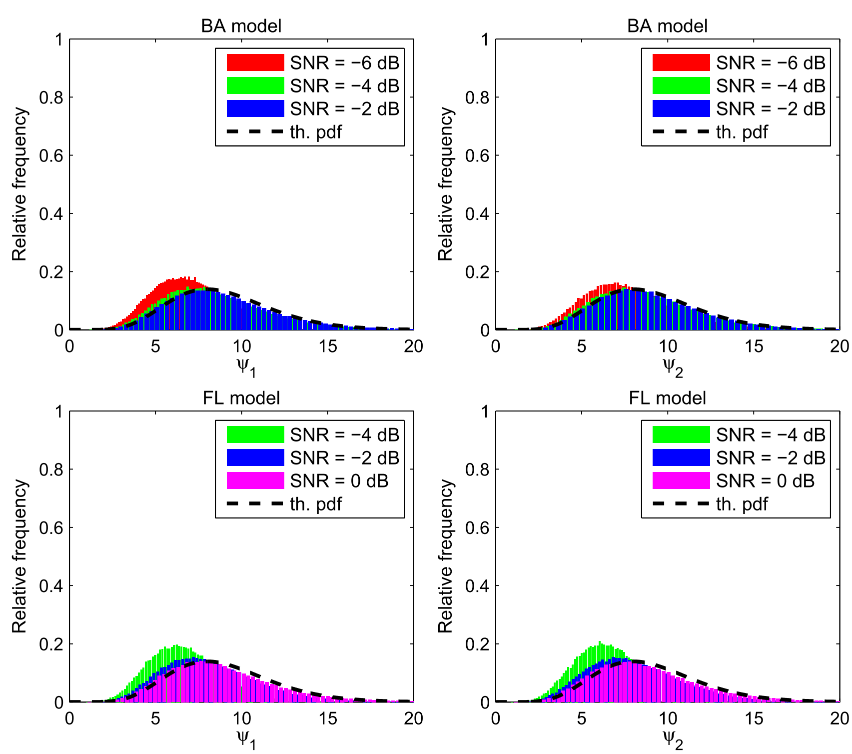

Fig. 6. TR-MUSIC null-spectrum in *usual* setup: empirical pdf vs. SNR; theoretical (obtained via Eq. (26), in dashed black line) vs. simulated (MC-based) performance.

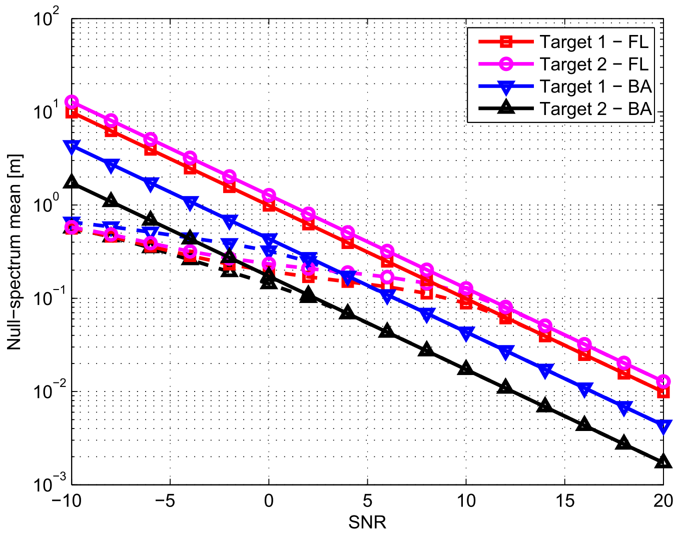

Fig. 7. TR-MUSIC null-spectrum in *sub-wavelength* setup: Mean vs. SNR; theoretical (obtained via Eq. (28), in solid lines) vs. simulated (MC-based) performance.

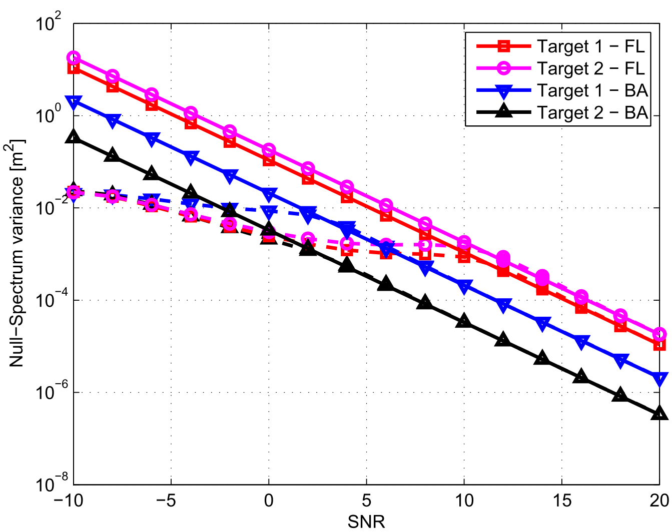

Fig. 8. TR-MUSIC null-spectrum in *sub-wavelength* setup: Variance vs. SNR; theoretical (obtained via Eq. (30), in solid lines) vs. simulated (MC-based) performance.

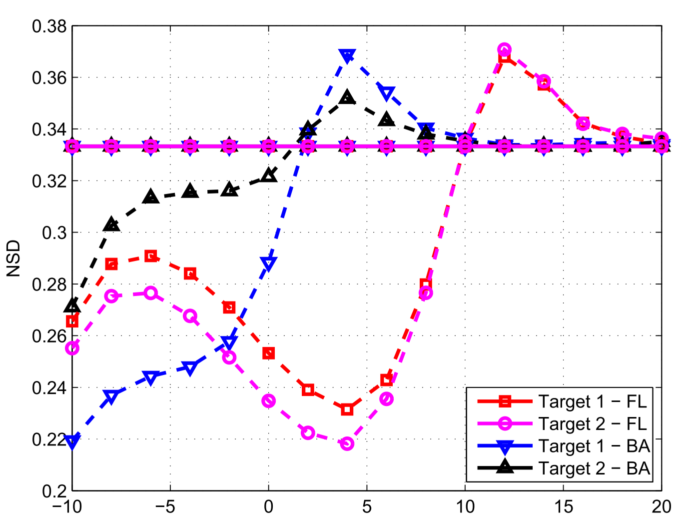

Fig. 9. TR-MUSIC null-spectrum in *sub-wavelength* setup: NSD vs. SNR; theoretical (obtained via Eq. (31), in solid lines) vs. simulated (MC-based) performance.

is higher than the corresponding value of the previous experiment, thus underlining the significant mutual scattering effect experienced in this case when considering FL model. From inspection of Figs. 7 and 8, it is apparent that a similar behavior as in the previous experiment can be observed, thus confirming the *general validity* of the obtained expressions of Sec. 3. Clearly, in the case of the NSD (cf. Fig. 9), the same value (i.e. $\mathrm{NSD}_k \approx 0.33$) as in the previous setup is attained. However, since the scatterers are closer, their relevant signatures (represented by the Green vector functions) will be very similar and thus a lower level of noise (viz. a higher SNR level) is required for the present analysis to apply. Indeed, the true pdf and the first two-order moments approach their asymptotic forms at SNR ≈ 14 dB, see e.g. Fig. 10, where the empirical pdf is shown against the theoretical pdf for three representative values (i.e. SNR $\in \{-5, 0, 5\}$ dB for BA scenario and SNR $\in \{0, 5, 10\}$ dB for FL scenario).

5. Concluding remarks

The present study provided a theoretical analysis of TR-MUSIC null-spectrum, focusing on a narrowband co-located multistatic setup. To accomplish the aforementioned task, we took advantage of a 1st order perturbation of the SVD of the noise-free MDM. More specifically, we demonstrated that its asymptotic (high-SNR) pdf is a scaled complex chi-square with a number of complex DOFs given by the dimension of the orthogonal subspace, that is $N - M$. The aforementioned result was also exploited to show that the asymptotic noisiness of the null-spectrum only depends on $(N - M)$. This finding holds independently on the peculiar scattering model being assumed. Finally, theoretical findings were confirmed in a 2D localization scenario by simulations.

Future studies will focus on (asymptotic) TR-MUSIC null-spectrum analysis in more advanced (and/or realistic) setups, such as non-colocated ones, where several TR-MUSIC spatial spectrum variants were proposed in the latter context [12]. Furthermore, wideband data, scatterers with finite extent, and mismatches in the array model will be analyzed. Similarly, propagation in random (non-homogeneous) media and clutter-dominated environments will be investigated as well.

Appendix

In order to demonstrate the result in Eq. (22), we first evaluate the covariance of $\boldsymbol{\xi}_k$ as (since the mean is null)

$$\boldsymbol{\Xi}_k \triangleq \mathbb{E}\left\{\boldsymbol{\xi}_k \boldsymbol{\xi}_k^\dagger\right\} = \boldsymbol{U}_n^\dagger \, \mathbb{E}\left\{\boldsymbol{W}\, \boldsymbol{t}_k \boldsymbol{t}_k^\dagger \, \boldsymbol{W}^\dagger\right\} \boldsymbol{U}_n\,, \tag{37}$$

where $\boldsymbol{t}_k \triangleq \boldsymbol{V}_s \, \boldsymbol{\Sigma}_s^{-1} \boldsymbol{U}_s^\dagger \, \bar{\boldsymbol{g}}(\boldsymbol{x}_k) \in \mathbb{C}^{N\times 1}$ is a *deterministic* vector. Then, we rewrite the expectation within Eq. (22) as follows:

$$\mathbb{E}\left\{\boldsymbol{W}\, \boldsymbol{t}_k \boldsymbol{t}_k^\dagger \, \boldsymbol{W}^\dagger\right\} = \sum_{m=1}^{N}\sum_{n=1}^{N} t_{k,m} t_{k,n}^* \, \mathbb{E}\left\{\boldsymbol{w}_m \boldsymbol{w}_n^\dagger\right\}\,, \tag{38}$$

where $\boldsymbol{w}_n$ denotes the nth column of $\boldsymbol{W}$. Similarly, the pseudo-covariance of $\boldsymbol{\xi}_k$ can be evaluated as:

$$\boldsymbol{\Psi}_k \triangleq \mathbb{E}\left\{\boldsymbol{\xi}_k \boldsymbol{\xi}_k^T\right\} = \boldsymbol{U}_n^\dagger \, \mathbb{E}\left\{\boldsymbol{W}\, \boldsymbol{t}_k \boldsymbol{t}_k^T \, \boldsymbol{W}^T\right\} \boldsymbol{U}_n^*\,, \tag{39}$$

where the expectation in the above expression is rewritten conveniently as:

$$\mathbb{E}\left\{\boldsymbol{W}\, \boldsymbol{t}_k \boldsymbol{t}_k^T \, \boldsymbol{W}^T\right\} = \sum_{m=1}^{N}\sum_{n=1}^{N} t_{k,m} t_{k,n} \, \mathbb{E}\left\{\boldsymbol{w}_m \boldsymbol{w}_n^T\right\}. \tag{40}$$

Since $\mathrm{vec}(\boldsymbol{W}) \sim \mathcal{N}_{\mathbb{C}}(\boldsymbol{0}_{N^2}, \sigma_w^2 \, \boldsymbol{I}_{N^2})$, the following properties hold:

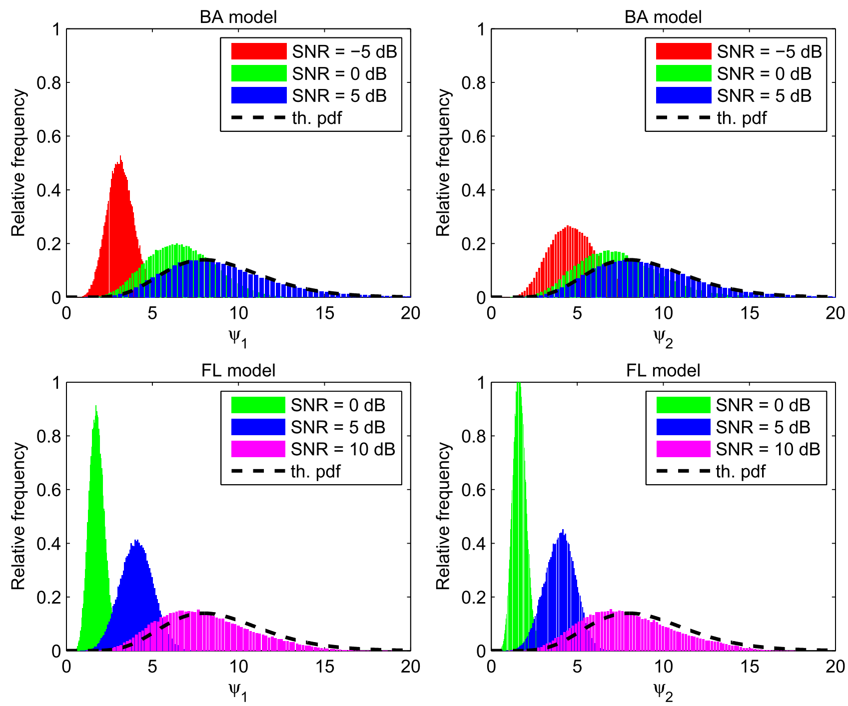

Fig. 10. TR-MUSIC null-spectrum in *sub-wavelength* setup: empirical pdf vs. SNR; theoretical (obtained via Eq. (26), in dashed black line) vs. simulated (MC-based) performance.

$$\mathbb{E}\{\boldsymbol{w}_n \boldsymbol{w}_m^\dagger\} = \delta(n-m)\,\sigma_w^2\,\boldsymbol{I}_N\,; \tag{41}$$

$$\mathbb{E}\{\boldsymbol{w}_n \boldsymbol{w}_m^T\} = \boldsymbol{0}_{N\times N}\,. \tag{42}$$

The aforementioned properties, when exploited in Eqs. (38) and (40), provide:

$$\mathbb{E}\left\{\boldsymbol{W}\,\boldsymbol{t}_k \boldsymbol{t}_k^\dagger\,\boldsymbol{W}^\dagger\right\} = \|\boldsymbol{t}_k\|^2\,\sigma_w^2\,\boldsymbol{I}_N\,; \tag{43}$$

$$\mathbb{E}\left\{\boldsymbol{W}\,\boldsymbol{t}_k \boldsymbol{t}_k^T\,\boldsymbol{W}^T\right\} = \boldsymbol{0}_{N\times N}\,. \tag{44}$$

Substituting (43) in Eq. (37) leads to the closed-form of covariance $\boldsymbol{\Xi}_k$

$$\boldsymbol{\Xi}_k = \boldsymbol{U}_n^\dagger\left(\|\boldsymbol{t}_k\|^2\,\sigma_w^2\,\boldsymbol{I}_N\right)\boldsymbol{U}_n, \tag{45}$$

$$= \|\boldsymbol{t}_k\|^2\,\sigma_w^2\,\boldsymbol{I}_{N-M}\,, \tag{46}$$

where we in last line we have exploited the fact that $\boldsymbol{U}_n$ is a *slice* of a *unitary matrix* (cf. Eq. (10)), that is $(\boldsymbol{U}_n^\dagger \boldsymbol{U}_n) = \boldsymbol{I}_{N-M}$. Finally, exploiting Eq. (44) into (39) provides $\boldsymbol{\Psi}_k = \boldsymbol{0}_{(N-M)\times(N-M)}$.

References

[1] M. Fink, Time-reversal mirrors, J. Phys. D, Appl. Phys. 26 (9) (1993) 1333.
[2] D. Cassereau, M. Fink, Time-reversal of ultrasonic fields. III. Theory of the closed time-reversal cavity, IEEE Trans. Ultrason. Ferroelectr. Freq. Control 39 (5) (1992) 579–592.
[3] J.W. Odendaal, E. Barnard, C.W.I. Pistorius, Two-dimensional superresolution radar imaging using the MUSIC algorithm, IEEE Trans. Antennas Propag. 42 (10) (1994) 1386–1391.
[4] G. Micolau, M. Saillard, P. Borderies, DORT method as applied to ultrawideband signals for detection of buried objects, IEEE Trans. Geosci. Remote Sens. 41 (8) (2003) 1813–1820.
[5] L. Li, W. Zhang, F. Li, A novel autofocusing approach for real-time through-wall imaging under unknown wall characteristics, IEEE Trans. Geosci. Remote Sens. 48 (1) (2010) 423–431.
[6] M.D. Hossain, A.S. Mohan, M.J. Abedin, Beamspace time-reversal microwave imaging for breast cancer detection, Antennas Wirel. Propag. Lett. 12 (2013) 241–244, http://dx.doi.org/10.1109/LAWP.2013.2247018.
[7] A.E. Fouda, F.L. Teixeira, Ultra-wideband microwave imaging of breast cancer tumors via Bayesian inverse scattering, J. Appl. Phys. 115 (6) (2014) 064701.
[8] M.D. Hossain, A.S. Mohan, Coherent time reversal microwave imaging for the detection and localization of breast tissue malignancies, Radio Sci. 50 (2) (2015) 87–98.
[9] T. Yin, F.H. Ali, C.C. Reyes-Aldasoro, A robust and artifact resistant algorithm of ultrawideband imaging system for breast cancer detection, IEEE Trans. Biomed. Eng. 62 (6) (2015) 1514–1525.
[10] C. Prada, S. Manneville, D. Spoliansky, M. Fink, Decomposition of the time reversal operator: detection and selective focusing on two scatterers, J. Acoust. Soc. Am. 99 (4) (1996) 2067–2076.
[11] A.J. Devaney, Time reversal imaging of obscured targets from multistatic data, IEEE Trans. Antennas Propag. 53 (5) (2005) 1600–1610.
[12] E.A. Marengo, F.K. Gruber, Subspace-based localization and inverse scattering of multiply scattering point targets, EURASIP J. Adv. Signal Process. (2007) 1–16.
[13] R. Solimene, A. Dell'Aversano, Some remarks on time-reversal MUSIC for two-dimensional thin PEC scatterers, IEEE Geosci. Remote Sens. Lett. 11 (6) (2014) 1163–1167, http://dx.doi.org/10.1109/LGRS.2013.2288516.
[14] E.A. Marengo, F.K. Gruber, F. Simonetti, Time-reversal MUSIC imaging of extended targets, IEEE Trans. Image Process. 16 (8) (2007) 1967–1984.
[15] H. Krim, M. Viberg, Two decades of array signal processing research: the parametric approach, IEEE Signal Process. Mag. 13 (4) (1996) 67–94.
[16] R. Schmidt, Multiple emitter location and signal parameter estimation, IEEE Trans. Antennas Propag. 34 (3) (1986) 276–280.
[17] M. Kaveh, A. Barabell, The statistical performance of the MUSIC and the minimum-norm algorithms in resolving plane waves in noise, IEEE Trans. Acoust. Speech Signal Process. 34 (2) (1986) 331–341.
[18] P. Stoica, A. Nehorai, MUSIC, maximum likelihood, and Cramér-Rao bound, IEEE Trans. Acoust. Speech Signal Process. 37 (5) (1989) 720–741.
[19] P. Stoica, A. Nehorai, MUSIC, maximum likelihood, and Cramér-Rao bound: further results and comparisons, IEEE Trans. Acoust. Speech Signal Process. 38 (12) (1990) 2140–2150.
[20] F. Li, R.J. Vaccaro, Analysis of min-norm and MUSIC with arbitrary array geometry, IEEE Trans. Aerosp. Electron. Syst. 26 (6) (1990) 976–985.
[21] B. Porat, B. Friedlander, Analysis of the asymptotic relative efficiency of the MUSIC algorithm, IEEE Trans. Acoust. Speech Signal Process. 36 (4) (1988) 532–544.
[22] A.L. Swindlehurst, T. Kailath, A performance analysis of subspace-based methods in the presence of model errors, Part I: the MUSIC algorithm, IEEE Trans. Signal Process. 40 (7) (1992) 1758–1774.
[23] B. Friedlander, A sensitivity analysis of the MUSIC algorithm, IEEE Trans. Acoust. Speech Signal Process. 38 (10) (1990) 1740–1751.
[24] A. Ferréol, P. Larzabal, M. Viberg, On the asymptotic performance analysis of subspace DOA estimation in the presence of modeling errors: case of MUSIC, IEEE Trans. Signal Process. 54 (3) (2006) 907–920.
[25] A. Ferréol, P. Larzabal, M. Viberg, On the resolution probability of MUSIC in presence of modeling errors, IEEE Trans. Signal Process. 56 (5) (2008) 1945–1953.

[26] A. Ferréol, P. Larzabal, M. Viberg, Statistical analysis of the MUSIC algorithm in the presence of modeling errors, taking into account the resolution probability, IEEE Trans. Signal Process. 58 (8) (2010) 4156–4166.
[27] D. Ciuonzo, G. Romano, R. Solimene, On MSE performance of time-reversal MUSIC, in: IEEE 8th Sensor Array and Multichannel Signal Processing Workshop, SAM, 2014, pp. 13–16.
[28] D. Ciuonzo, G. Romano, R. Solimene, Performance analysis of time-reversal MUSIC, IEEE Trans. Signal Process. 63 (10) (2015) 2650–2662.
[29] G. Shi, A. Nehorai, Maximum likelihood estimation of point scatterers for computational time-reversal imaging, Commun. Inf. Syst. 5 (2) (2005) 227–256.
[30] D. Ciuonzo, On Time-Reversal imaging by statistical testing, IEEE Signal Process. Lett. 24 (7) (2017) 1024–1028.
[31] G. Shi, A. Nehorai, Cramér-Rao bound analysis on multiple scattering in multistatic point-scatterer estimation, IEEE Trans. Signal Process. 55 (6) (2007) 2840–2850.
[32] J. Choi, I. Song, Asymptotic distribution of the MUSIC null spectrum, IEEE Trans. Signal Process. 41 (2) (1993) 985–988.
[33] F. Li, H. Liu, R.J. Vaccaro, Performance analysis for DOA estimation algorithms: unification, simplification, and observations, IEEE Trans. Aerosp. Electron. Syst. 29 (4) (1993) 1170–1184.
[34] Z. Xu, Perturbation analysis for subspace decomposition with applications in subspace-based algorithms, IEEE Trans. Signal Process. 50 (11) (2002) 2820–2830.
[35] G.W. Stewart, Error and perturbation bounds for subspaces associated with certain eigenvalue problems, SIAM Rev. 15 (4) (1973) 727–764.
[36] D.S. Bernstein, Matrix Mathematics: Theory, Facts, and Formulas, Princeton University Press, 2009.
[37] H.B. Lee, M.S. Wengrovitz, Statistical characterization of the MUSIC null spectrum, IEEE Trans. Signal Process. 39 (6) (1991) 1333–1347.
[38] M. Davy, J.-G. Minonzio, J. de Rosny, C. Prada, M. Fink, Influence of noise on subwavelength imaging of two close scatterers using time reversal method: theory and experiments, Prog. Electromagn. Res. 98 (2009) 333–358.

Domenico Ciuonzo was born in Aversa, Italy, on June 29, 1985. He received the B.Sc. and M.Sc. (summa cum laude) degrees in computer engineering and the Ph.D. degree from the Second University of Naples, Aversa, Italy, in 2007, 2009, and 2013, respectively.

In 2011, he was involved in the Visiting Researcher Programme of NATO CMRE, La Spezia, Italy. In 2012, he was a Visiting Scholar with the ECE Department, University of Connecticut, Storrs, CT, USA. In 2015 and 2016, he held visiting appointments at the Department of Electronics and Telecommunications, Norwegian University of Science and Technology, Trondheim, Norway. From 2014 to 2016, he was a Post-Doctoral Researcher with DIETI, University of Naples, Federico II, Italy. From 2017, he is a Researcher at NM2 s.r.l., Naples, Italy.

His reviewing activity was recognized by the IEEE Communications Letters and the IEEE Transactions on Communications, which nominated him Exemplary Reviewer, in 2013 and 2014, respectively. Since 2016, he is an IEEE Senior Member. Since 2014, he has served as Associate Editor for different journals of IEEE, IET and Inderscience. Additionally, from 2017, he serves as Technical (Area) Editor for the IEEE Transactions on Aerospace and Electronic Systems.

His research interests fall within the areas of data fusion, statistical signal processing, machine learning and wireless sensor networks.

Pierluigi Salvo Rossi was born in Naples, Italy, on April 26, 1977. He received the "Laurea" degree in telecommunications engineering (summa cum laude) and the Ph.D. degree in computer engineering, in 2002 and 2005, respectively, both from the University of Naples "Federico II", Naples, Italy.

From 2005 to 2008, he worked as a postdoc at the Department of Computer Science and Systems, University of Naples "Federico II", Naples, Italy, at the Department of Information Engineering, Second University of Naples, Aversa (CE), Italy, and at the Department of Electronics and Telecommunications, Norwegian University of Science and Technology, Trondheim, Norway.

From 2008 to 2014, he was an Assistant Professor (tenured in 2011) in telecommunications at the Department of Industrial and Information Engineering, Second University of Naples, Aversa (CE), Italy.

From 2014 to 2016, he was an Associate Professor in signal processing with the Department of Electronics and Telecommunications, Norwegian University of Science and Technology, Trondheim, Norway.

Since 2016 he is a Full Professor in signal processing with the Department of Electronic Systems, Norwegian University of Science and Technology, Trondheim, Norway.

He held visiting appointments at the Department of Electrical and Computer Engineering, Drexel University, Philadelphia, PA, US, at the Department of Electrical and Information Technology, Lund University, Lund, Sweden, at the Department of Electronics and Telecommunications, Norwegian University of Science and Technology, Trondheim, Norway, and at the Excellence Center for Wireless Sensor Networks (WISENET), Uppsala University, Uppsala, Sweden.

He is an IEEE Senior Member and serves as Senior Editor for the IEEE Communications Letters (since 2016) and Associate Editor for the IEEE Transactions on Wireless Communications (since 2015). He was Associate Editor for the IEEE Communications Letters (from 2012 to 2016).

His research interests fall within the areas of communications and signal processing.